Applied Catalysis B: Environmental 129 (2013) 375–381

Contents lists available at SciVerse ScienceDirect

Applied Catalysis B: Environmental

journal homepage: www.elsevier.com/locate/apcatb

Enhancement of oxygen reduction reaction on PtAu nanoparticles via CO induced surface Pt enrichment

Hee-Young Park[a,b,1,2], Tae-Yeol Jeon[a,1], Jong Hyun Jang[b,2], Sung Jong Yoo[b,2], Kwang-Hyun Choi[a,1], Namgee Jung[a,b,1,2], Yung-Hoon Chung[a,1], Minje Ahn[a,1], Yong-Hun Cho[c,3], Kug-Seung Lee[a,1], Yung-Eun Sung[a,*]

[a] World Class University (WCU) Program of Chemical Convergence for Energy & Environment (C2E2), School of Chemical & Biological Engineering, Seoul National University, Seoul 151-744, Republic of Korea
[b] Fuel Cell Research Center, Korea Institute of Science and Technology, 39-1 Hawolgok-dong, Seoul 136-791, Republic of Korea
[c] School of Advanced Materials Engineering, Kookmin University, Seoul 136-702, Republic of Korea

ARTICLE INFO

Article history:
Received 26 March 2012
Received in revised form
22 September 2012
Accepted 24 September 2012
Available online 2 October 2012

Keywords:
Polymer electrolyte membrane fuel cell
Electrocatalysis
PtAu
Surface segregation
Pt enrichment
Oxygen reduction reaction

ABSTRACT

To investigate the enhancement of the oxygen reduction reaction (ORR) activity on a carbon-supported PtAu alloy nanoparticle catalyst, the catalyst was subject to heat treatment at 423 K under a CO or Ar atmosphere. The surface composition was analyzed by XPS and the composition was shown to increase from 66 ± 2% (PtAu-AP) to 74 ± 2% (PtAu-CO) after heat treatment under a CO atmosphere, which was confirmed by electrochemical techniques, while the bulk composition was invariant at 55%. For the oxygen reduction reaction (ORR), the mass activity of PtAu-CO increased by 75.6% (33.2 A/g_{Pt}) when compared to that of PtAu-AP (18.9 A/g_{Pt}). Since the increase in EAS was only 15.8%, it was concluded that the specific activity was enhanced by 52.6% due to surface Pt segregation after heat treatment under a CO atmosphere. The enhanced specific activity was attributed to the reduced OH adsorption energy which was characterized by measuring the potential of total zero charge. The weaker OH adsorption was resulted from the higher Pt/Au ratio at the surface layers.

1. Introduction

Polymer electrolyte membrane fuel cells (PEMFCs) are believed to be the future source of electric power generation due to their high efficiency and low environmental impact. Despite significant advances in fuel cell technology, the high material cost of Pt catalysts is one of the main issues limiting commercialization of PEMFC. Pt based late transition metal alloys (PtTM) have been investigated with the goal of decreasing the Pt load. Stamekovic et al. reported that the Pt_3Ni_1 (1 1 1) surface has a 10-fold higher activity compared with Pt (1 1 1) due to a weaker OH adsorption energy, which results from the down shift of the d-band center [1]. Numerous PtTM nanoparticle catalysts have been used to improve the ORR activity [2–6], but the fast dissolution of "TM" results in a significant decrease in activity during fuel cell operation [7–9]. Thus, there is a need to develop durable as well as highly efficient electrocatalysts.

Due to the excellent intrinsic stability of Au [8], several studies have developed and analyzed Pt–Au electrocatalysts, such as PtAu alloy or Pt thin films on Au substrate, for fuel cell applications, including the oxygen reduction reaction (ORR) [10–12], formic acid oxidation [13–17], and methanol oxidation [15–18]. Pt–Au nanoparticles often showed enhanced ORR compared with Pt nanoparticles with weaker OH adsorption due to the contraction strain effect [19–25], while, in bulk material, Pt–Au has lower activity due to the lattice mismatch between Pt and Au (4.1%) [26,27]. However, ORR activity on PtAu alloy nanoparticles are lower than that on PtTM nanoparticles and improving the ORR activity of PtAu nanoparticles is still of significant importance. There are two different ways to increase the ORR activity of PtAu nanoparticles. One is to reduce the OH adsorption energy by modifying the electronic structure of PtAu nanoparticles, where the OH adsorption is stronger than optimum [28]. Another is to increase the number of active sites for ORR by controlling the surface composition.

CO induced surface segregation is an attractive strategy to improve the ORR activity of PtAu alloy nanoparticles, since the electronic structure and surface composition can be simultaneously modified. CO induced segregation was predicted by Greeley and

* Corresponding author. Tel.: +82 2 880 1889; fax: +82 2 880 1604.
E-mail addresses: jhjang@kist.re.kr (J.H. Jang), yhun00@kookmin.ac.kr (Y.-H. Cho), ysung@snu.ac.kr (Y.-E. Sung).
[1] Tel.: +82 2 880 1889; fax: +82 2 880 1604.
[2] Tel.: +82 2 958 5287; fax: +82 2 958 5199.
[3] Tel.: +82 2 910 5672; fax: +82 2 910 5674.

0926-3373/$ – see front matter © 2012 Elsevier B.V. All rights reserved.
http://dx.doi.org/10.1016/j.apcatb.2012.09.041

Mavrikakis via computational simulations for various combinations of metals [29]. To the best of our knowledge, there has only been one report that examined the relationship between CO induced surface segregation during thermal treatment and ORR activity. Mayrhofer et al. reported that thermal CO annealing could improve ORR mass activity of Pt–Co/C by a factor of ~3 when compared with untreated Pt–Co nanoparticles in alkaline media, but the specific activity and surface property changes during CO annealing was not examined [30]. Investigating the qualitatively changes of surface properties and ORR activity of PtAu nanoparticles during CO exposure will allow us to better understand the effect of CO induced segregation on the ORR activity and could help improve the ORR activity of Pt alloy nanoparticles. Core–shell structured Au–Pt nanoparticles with a Pt monolayer are the most efficient way to achieve 100% utilization and strong electronic modification of Pt, but have been prepared using an electrochemical method, which is not suitable for mass production. Thus, CO induced segregation could provide a practical way to increase Pt utilization and the specific activity of PtAu alloy nanoparticles. Therefore, improving our understanding of PtAu nanoparticle surfaces during CO induced Pt enrichment is expected to help overcoming the technical barriers; the sluggish ORR activity on Pt and instability of PtTM catalysts.

Here, we demonstrated enrichment of surface Pt concentrations in PtAu nanoparticles under a CO atmosphere, which enhanced the ORR activity. Pt enrichment and ORR activity was characterized by X-ray photoelectron spectroscopy (XPS) and electrochemical techniques. In addition, comparison of surface Pt concentration and activity changes of PtAu nanoparticles during CO induced segregation allowed us to investigate the relationship between surface properties, surface atomic composition and OH adsorption strength, and ORR activity with little changes in total atomic composition, crystalline structure and size of PtAu nanoparticles.

2. Experimental

2.1. Synthesis

All aqueous solutions were made with deionized (DI) water, which was further purified using a Mili-Q system (18.2 MΩ cm; Millipore, Bedford, MA, USA). The following chemicals were obtained from Sigma–Aldrich (St. Louis, MO, USA) and were used without further purification: $HAuCl_4{\cdot}3H_2O$, $H_2PtCl_6{\cdot}xH_2O$, $Na_3C_6H_5O_7{\cdot}2H_2O$, $HClO_4$, and $NaBH_4$.

Carbon supported PtAu nanoparticle catalysts (40 wt% PtAu/C) were prepared by modifying the method from our previous work [14]. Briefly, an appropriate amount of Pt salt (0.128 mmol), Au salt (0.128 mmol), and sodium citrate (0.068 mmol) was dissolved in 800 ml of DI water. Under vigorous stirring, an aqueous solution of sodium citrate (0.034 mmol) and sodium borohydide (2.64 mmol) was quickly added to the precursor solution. The color of the solution immediately changed from transparent yellow to translucent dark brown, indicating colloid formation. After thirty minutes, 0.075 g of Vulcan-XC72 (CABOT) was added to the colloid solution and stirred for 12 h. 200 ml of a 0.2 M $HClO_4$ solution was then added to the colloid solution. The mixture was filtered and washed with a copious amount of water. The catalyst was dried at room temperature and denoted as PtAu-AP. The surface segregation process was conducted using a tube furnace at 423 K for 1 h under a CO (99.9%) or Ar (99.999%) atmosphere to achieve a Pt or Au segregated surface, which were denoted as PtAu-CO and PtAu-Ar, respectively. The CO or Ar flow during surface segregation was 500 $cm^3\ min^{-1}$. A schematic representation of the selective surface segregation of Pt or Au in PtAu nanoparticles is shown in Fig. 1.

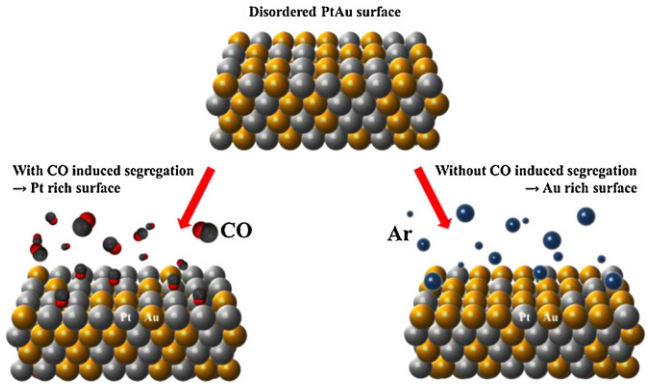

Fig. 1. Scheme representing selective segregation of Pt (left) or Au (right) under a CO or Ar atmosphere, respectively.

A commercial 40 wt% Pt/C catalyst (Johnson Matthey) was used as the pure Pt nanoparticle catalyst in the XRD and XPS analysis. For the pure Au nanoparticle catalyst, 30 wt% Au/C was prepared with Au colloid as described previously [31–34]. Briefly, the Au colloid was prepared by reducing the aqueous solution of the Au salt with $NaBH_4$ in the presence of sodium citrate. The colloid was mixed with carbon and stirred for 24 h. The suspension was filtered and washed with copious amount of water, and dried under ambient air.

2.2. Characterization and measurements

TEM images were taken using a JEM-2010 (JEOL Ltd., Tokyo, Japan) microscope at an acceleration voltage of 200 kV. A D-MAX2500 diffractometer (Rigaku Corp., The Woodlands, TX, USA) was used to obtain XRD patterns at a gun power of 8 kW. The XPS analysis was performed with a Theta Probe (Thermo Electron Corp., Waltham, MA, USA) at the Korea Basic Science Institute. Electrochemical measurements were conducted in a standard three-compartment electrochemical cell using a rotating disk electrode system (Eco Chemie BV). A catalyst-coated glassy carbon (GC, 5 mm diameter) substrate, GC rod, and saturated calomel electrodes were used as working, counter, and reference electrodes, respectively. However, all potentials were calibrated using a homemade reversible hydrogen electrode (RHE) and reported with respect to the RHE. The reference was separated from the working electrode compartment by an electrolyte bridge to avoid chloride contamination. Ar-purged 0.1 M $HClO_4$ was used for all electrochemical measurements, except for the ORR polarization measurements. Cyclic voltammetry was conducted at a scan rate of 20 $mV\ s^{-1}$. Before the CV measurement, potential cycling in the range from 0 V to 0.4 V was performed to obtain a stable voltammogram. The cyclic voltammograms were reproducible with a deviation in the hydrogen desorption charge density of ~3%. ORR polarization was obtained in a O_2 saturated 0.1 M $HClO_4$ solution at a rotating rate of 1600 rpm and a scan rate of 5 $mV\ s^{-1}$ [35]. All electrochemical measurements were conducted isothermally at 20 ± 0.5 °C.

Potential of zero total charge (pztc) was calculated from the charge contribution of hydrogen desorption, which were displaced by CO [36,37]. Briefly, CO was adsorbed onto the electrode at 0.104 V, where the specially adsorbed hydrogen is the dominant ion species and the desorption charge due to the adsorption of CO was recorded. The potential having an identical charge density, pztc, form CO-displacement and integration of cyclic voltammogram was determined.

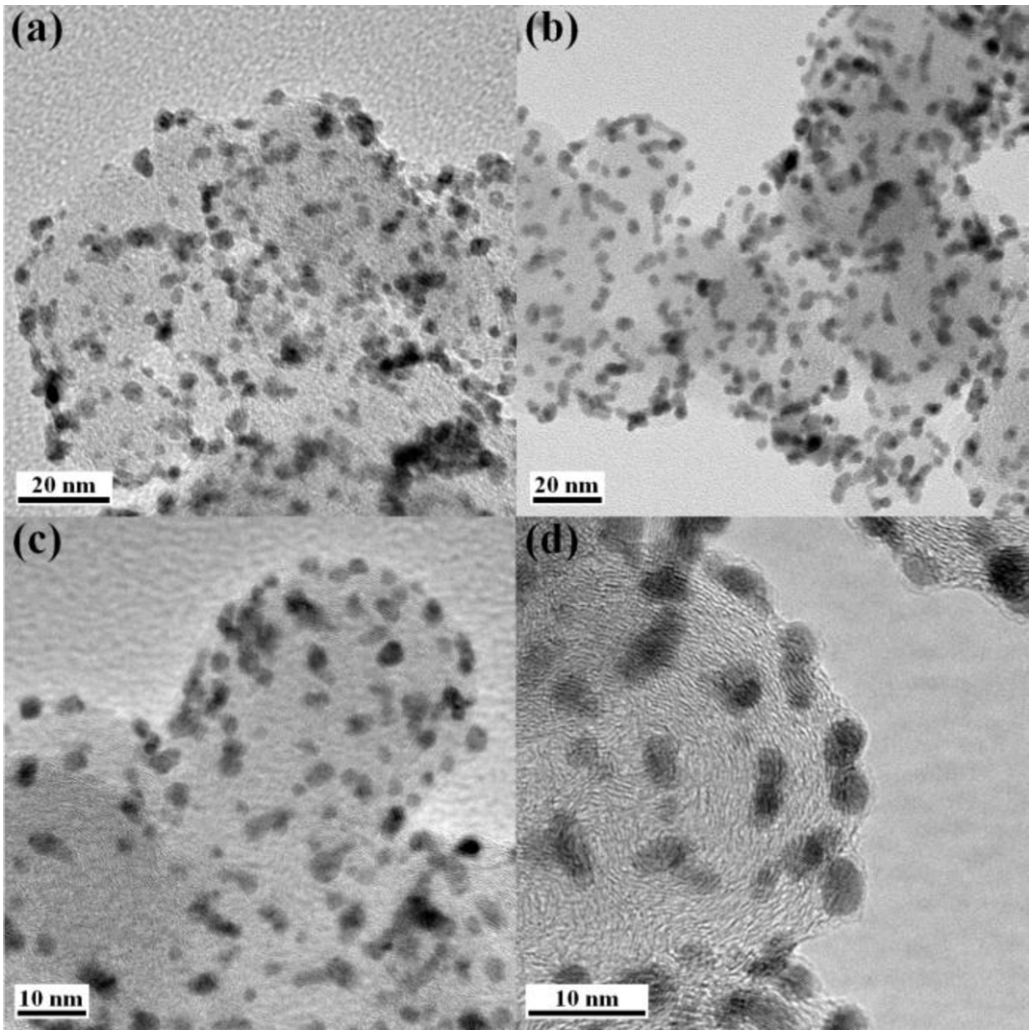

Fig. 2. Transmission electron microscopy images of: (a) PtAu-AP, (b) PtAu-Ar, (c) PtAu-CO and (d) a magnified image of PtAu-CO.

3. Results and discussion

3.1. Characterization of the PtAu nanoparticles

Fig. 1 shows a schematic of surface enrichment during CO or Ar exposure. A Pt rich surface could be achieved under a CO atmosphere since the CO adsorption energy is much higher for Pt (−1.35 eV) compared to the Au (−0.35 eV) [22,29,38,39], while Au segregation is favored under an Ar atmosphere due to the lower surface free-energy of Au (1.41 J m^{-2}) than that of Pt (2.34 J m^{-2}) [40].

The particle size of the PtAu nanoparticles was investigated using TEM and XRD. The average size of the nanoparticles from TEM were 1.86 ± 0.31 nm, 2.00 ± 0.21 nm, and 1.96 ± 0.29 nm for PtAu-AP, PtAu-CO, and PtAu-Ar, respectively (Fig. 2 and supporting information). Little aggregation or crystalline growth (~7.5%) of the nanoparticles was observed after heat treatment. The XRD patterns of the PtAu/C catalysts are presented in Fig. 3 (Pt/C and Au/C were presented as a comparison). The crystalline sizes of PtAu nanoparticles determined using the line broadening of (2 2 0) peak were 2.2 nm, 2.4 nm, and 2.2 nm for PtAu-AP, PtAu-CO, and PtAu-Ar respectively, which was in good agreement with the TEM analysis. The crystalline structure of the PtAu nanoparticles hardly changed during heat treatment, since surface segregation is expected to occur near the surface few layers (Fig. 4).

The XRD peak of PtAu nanoparticles suggested that the nanoparticles had typical fcc structure. The lattice constants of the PtAu nanoparticles (PtAu-AP: 3.99 Å, PtAu-CO: 4.00 Å, PtAu-Ar: 4.01 Å) were very similar to that of PtAu alloy (4.00), which was calculated

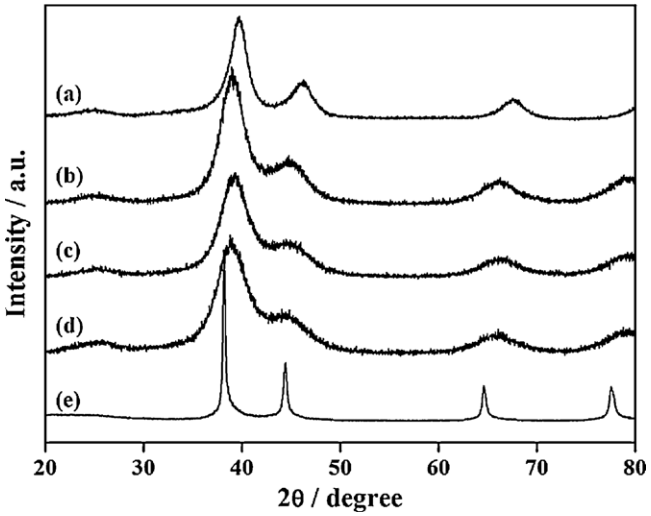

Fig. 3. X-ray diffraction of: (a) commercial Pt/C, (b) PtAu-CO, (c) PtAu-Ar, (d) PtAu-AP, and (e) Au/C.

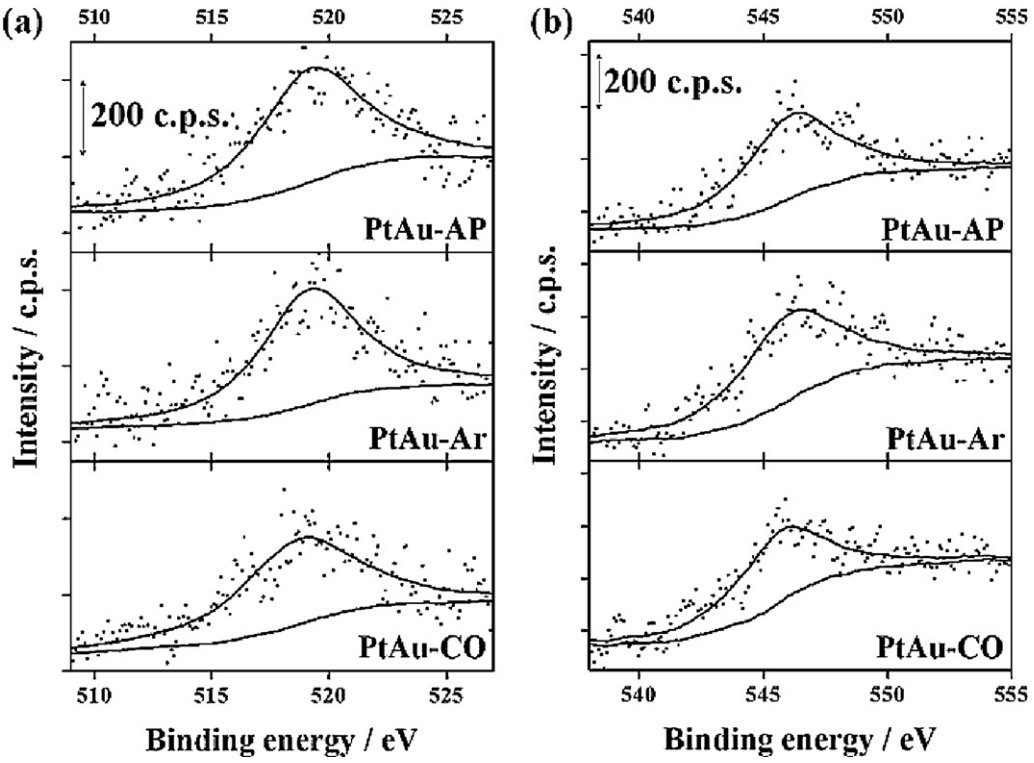

Fig. 4. X-ray photoelectron spectra of PtAu nanoparticles from Pt $4p_{3/2}$ (a) and Au $4p_{3/2}$ (b).

by Vegard's law using the lattice constants of Au (4.10 Å) and Pt (3.91 Å) nanoparticles. As shown in Fig. 5, the binding energy of Pt 4f in the PtAu nanoparticles (70.7 eV) shifted to negative values when compared with Pt/C (71.4 eV). PtAu nanoparticles showed a lower binding energy of Au 4f (83.6 eV) when compared with that of Au/C (84.2 eV) (see supporting information). This observed binding energy shift was in good agreement with previous reports, and suggested that our catalysts were alloy nanoparticles [41,42].

The bulk composition of PtAu nanoparticles were determined from the intensity ratio of Pt 4f and Au 4f XPS (Fig. 6), since the

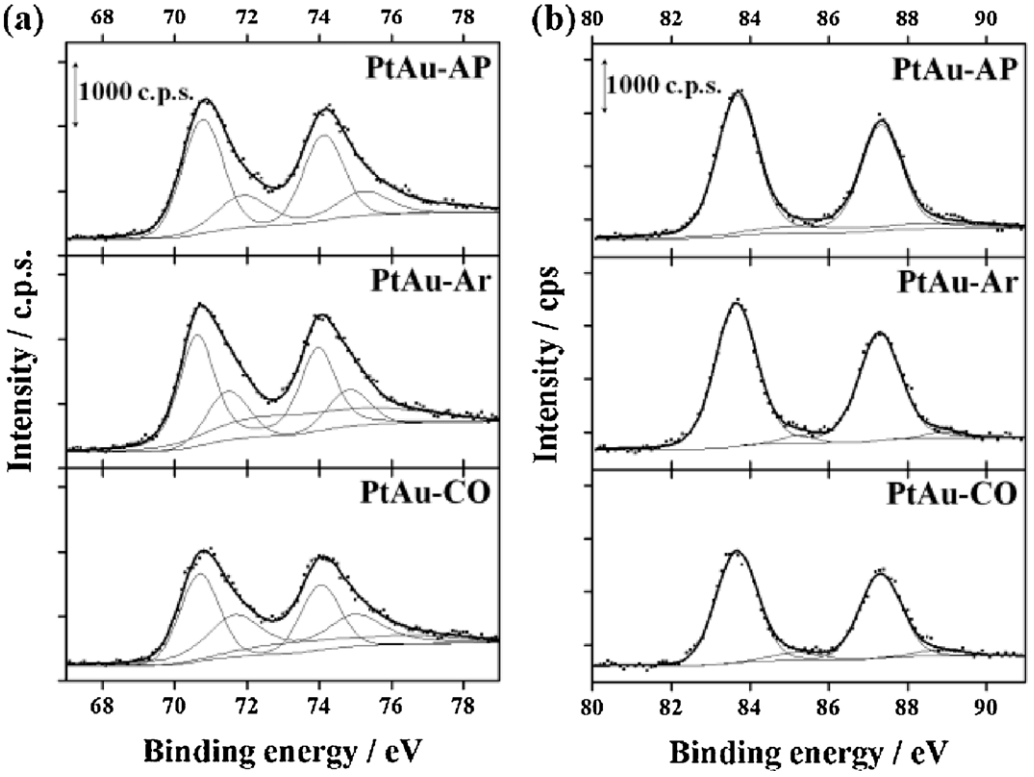

Fig. 5. X-ray photoelectron spectra of PtAu nanoparticles from Pt 4f (a) and Au 4f (b).

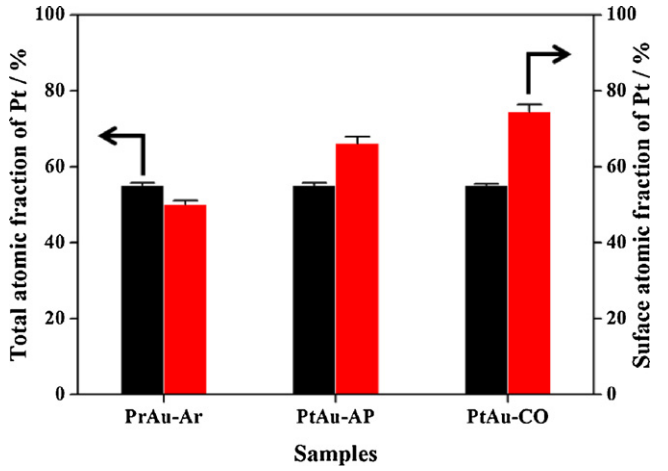

Fig. 6. Total (black, left) and surface (red, right) atomic fraction of Pt determined by intensities of X-ray photoelectron spectra in the 4f and $4p_{3/2}$ regions, respectively. (For interpretation of the references to color in the artwork, the reader is referred to the web version of the article.)

mean free path of the photoelectron is >20 Å with high kinetic energies (>1000 eV) [43]. The XPS intensity ratios of Pt and Au were obtained from the average of 5 different samplings of a catalyst to confirm that the compositions of the catalysts were uniform. The bulk fraction of Pt (# of Pt atoms/# of Pt and Au atoms in PtAu nanoparticles) was 55.1 ± 0.5% in PtAu-AP. The higher Pt atomic fraction of PtAu-AP than that of precursor solution (0.128 mmol for Pt and Au) likely originated from the higher Pt fraction near the surface region [44,45]. The bulk atomic fraction of Pt hardly changed during heat treatment under the Ar (55.2 ± 0.5%) or CO (55.2 ± 0.3%) atmosphere.

The surface atomic fraction of Pt to total metal was determined from the XPS intensity of Pt $4p_{3/2}$ and Au $4P_{3/2}$ with correction of the photoelectron cross section [41,46]. The mean free path of the photoelectrons Pt $4p_{3/2}$ and Au $4p_{3/2}$ were approximately 14 Å [43,47]. The surface atomic fraction of Pt calculated from the XPS intensity ratio of Pt $4p_{3/2}$ and Au $4p_{3/2}$ was 74 ± 2%, which corresponded to 1.12 times that of the PtAu-AP (66 ± 2%), whereas the surface atomic fraction of Pt in the PtAu-Ar was only 50 ± 1%.

In addition, the surface fraction of Pt was electrochemically characterized by comparing the ratio between electrochemical surface area (ECA) of Pt and Au deduced from the hydrogen desorption on Pt ($Q_{H,Pt}$) and reduction charge of Au surface oxide ($Q_{OH,Au}$), respectively. The electrochemical surface area of Au (ECA_{Au}) was determined from the CV of the catalysts between 0.05 V and 1.50 V (Fig. 7a). This was used because Au has a characteristic reduction peak at ca. 1.3 V with a charge density of 400 μC cm^{-2}. The ECA_{Au} decreased by 18.3% during CO exposure (PtAu-AP: 17.5 $m^2\ g_{Au}^{-1}$, PtAu-CO: 14.3 $m^2\ g_{Au}^{-1}$), but Ar treatment led to a 58.9% (27.8 $m^2\ g_{Au}^{-1}$) increase in ECA_{Au}. Since the CV measurement at >1.3 V could result in irreversible oxidation of Pt, the $Q_{H,Pt}$ was obtained from another CV measurement with an anodic limit of 1.00 V (Fig. S9). The ECA_{Pt} of PtAu-AP, PtAu-CO, and PtAu-Ar were 33.0 $m^2\ g_{Pt}^{-1}$, 38.2 $m^2\ g_{Pt}^{-1}$, and 31.5 $m^2\ g_{Pt}^{-1}$, respectively, based on the hydrogen desorption charge density on polycrystalline Pt (210 μC cm^{-2}). From the ECA_{Pt} and ECA_{Au}, the surface Pt fraction of PtAu-AP was determined to be 65.3%. The surface Pt fraction of PtAu-CO was 1.11 times higher (72.8%) than that of PtAu-AP, whereas the surface Pt fraction of PtAu-Ar was 53.1% (Fig. 7b). The surface Pt fractions form the ECA ratio were in good agreement with the results obtained from the XPS analysis, which indicate surface enrichment of Pt in the PtAu nanoparticles.

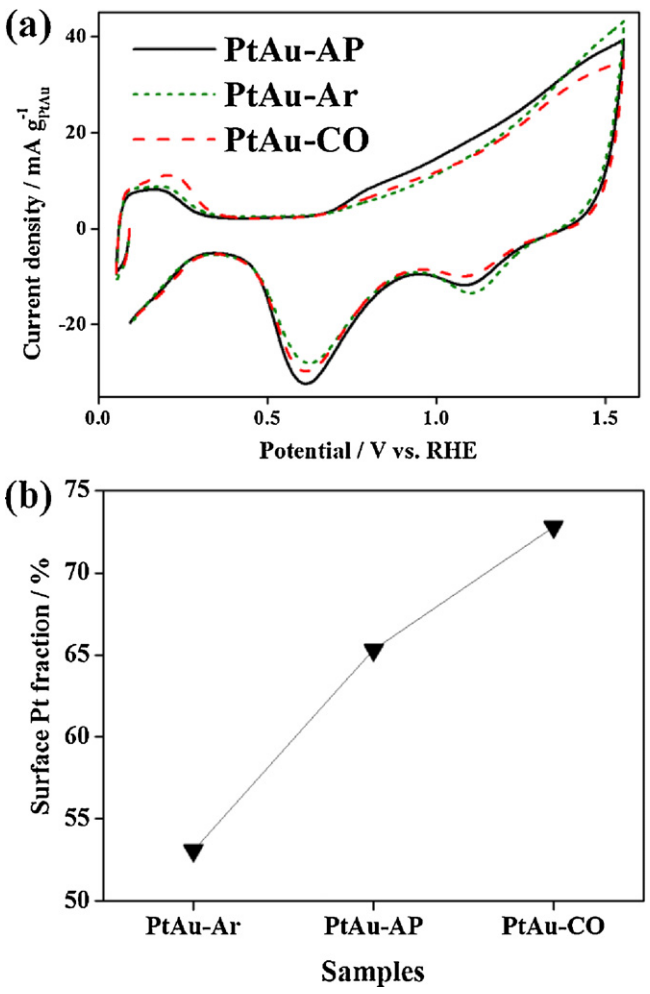

Fig. 7. (a) Cyclic voltammogram (potential range, 54–1554 mV) and (b) Pt surface atomic fraction in the PtAu nanoparticles.

3.2. Electrocatalytic activity for oxygen reduction reaction

As shown in the ORR polarization curves (Fig. 8), the half wave potential ($E_{1/2}$) of PtAu-CO (903 mV) was more positive compared

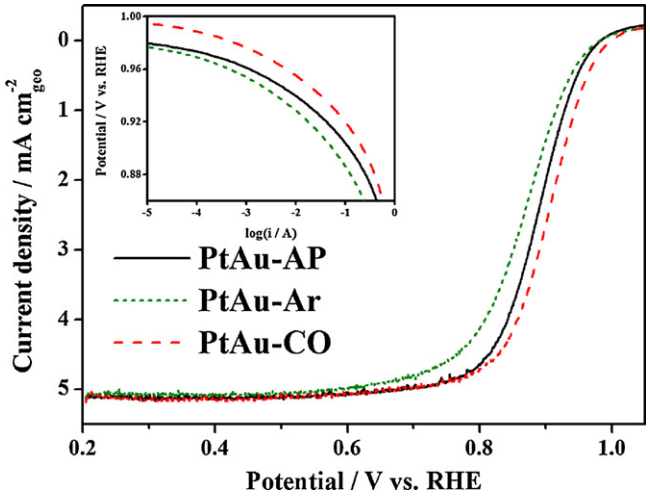

Fig. 8. Oxygen reduction reaction (ORR) polarization on PtAu-AP (black), PtAu-Ar (green), and PtAu-CO (red). Tafel plot of the ORR is presented in the inset. (For interpretation of the references to color in the artwork, the reader is referred to the web version of the article.)

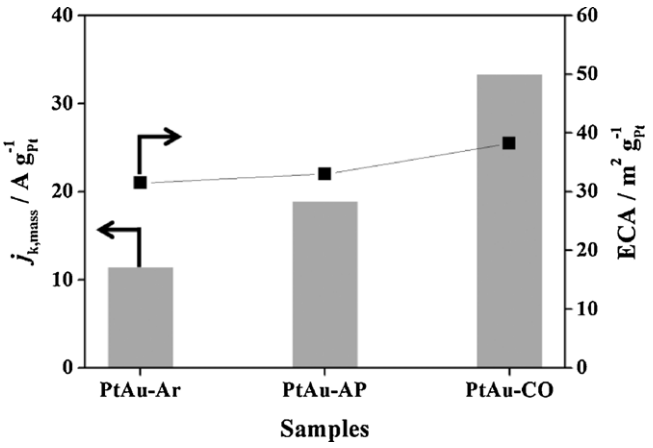

Fig. 9. Mass activity (bar, left) and specific area (square, right) of PtAu/C.

to the PtAu-AP (887 mV), demonstrating that the ORR activity was enhanced by the CO induced Pt segregation. When the ECA was increased from 33.0 m^2 g_{Pt}^{-1} (PtAu-AP) to 38.2 m^2 g_{Pt}^{-1} (PtAu-CO), the $E_{1/2}$ shift with a larger active Pt area was estimated to be +4.0 mV according to the relationship between ECA and $E_{1/2}$ suggested by Adzic et al. However, in this study, the experimental $E_{1/2}$ shift was as large as +16 mV, suggesting that the turnover frequency, current density normalized with respect to the ECA_{Pt} in electrocatalysis, was also enhanced, as well as the ECA, through the heat-treatment under the CO condition (Fig. 9).

From the polarization data, the mass activity was calculated to be 18.9 A g_{Pt}^{-1} (PtAu-AP), 33.2 A g_{Pt}^{-1} (PtAu-CO), and 11.4 A g_{Pt}^{-1} (PtAu-Ar), by using the Koutecky–Levich equation:

$$\frac{1}{i} = \frac{1}{i_k} + \frac{1}{i_{dl}}$$

where i is the measured current, i_k is measured kinetic current, and i_{dl} is diffusion limiting current [48]. The specific activity was determined by dividing i_k by the ECA_{Pt} values. As shown in Fig. 10, the specific activity of PtAu-CO (1.74 mA cm_{Pt}^{-2}) was 1.53 times higher than that of PtAu-AP (1.14 mA cm_{Pt}^{-2}), which was expected based on the large shift in the polarization curves. Since the ORR reaction on the Pt–Au alloy is limited by the desorption step of intermediate OH [49–51], it seems that the adsorption energy of OH decreased as a result of CO induced surface modification.

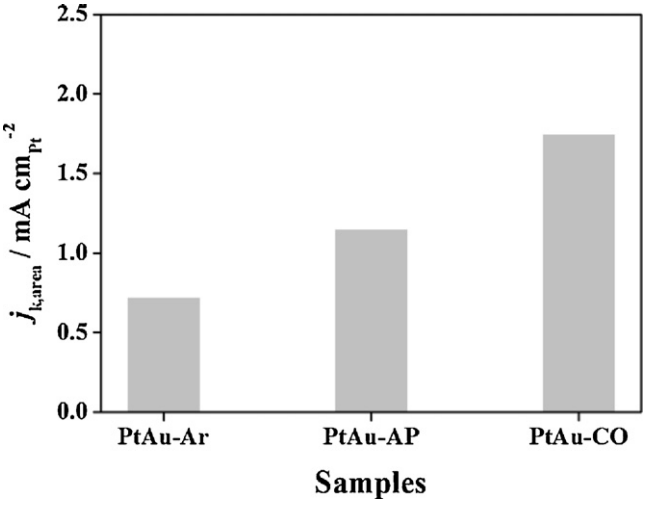

Fig. 10. Specific activity (i_k/ECA_{Pt} at 0.9 V) of PtAu/C.

To experimentally validate the change in OH adsorption energy, the pztc values were measured for each sample using the CO-displacement technique, which was suggested by Climent et al. [36]. Even though there exist hindrance by specific adsorption, Gómez et al. found that the pztc is linearly related to the work function level, which is directly connected to the adsorption strength of ions. Thus, the pztc by CO-displacement technique has been widely utilized to investigate adsorption energy of ions [52–58]. The pztc values of the Pt could be experimentally measured by finding the potential where the surface charge density of anions and cations is equal. The cationic contribution of surface charge could be calculated from the CV measurement, since the underpotentially deposited hydrogen is the dominant cationic species in the potential range of CO-displacement. The anionic contribution to the surface charge could be determined by subtracting the total surface charge collected during CO adsorption from the cationic surface charge, $Q_{H,Pt}$ above the CO adsorption potential (0.104 V). The experimental pztc values were more positive for PtAu-CO (221 mV) when compared to the PtAu-AP (209 mV), which clearly demonstrates that the OH adsorption became much weaker through the CO induced Pt segregation. The specific activity enhancement of 53% with a pztc increase of 12 mV seems to be reasonable, while the activity was reported to increase be a factor of 5 with a 35 mV pztc variation when the Pt nanoparticle size was increased (1 nm → 30 nm) [59]. Therefore, it can be summarized that the increased surface Pt fraction (65.3% → 72.8%) by CO heat treatment led to weaker OH adsorption, enhancing overall ORR activity, which is in consistent with the Pedersen et al.'s report, weaker OH adsorption energy with higher Pt fraction, for the PtAu monolayer on Pt(1 1 1) or Au(1 1 1) with various surface Pt fractions between 40% and 100% [60].

The comparison of the surface Pt concentration and ORR activity of PtAu nanoparticles during CO induced segregation allowed us to evaluate the enhanced ORR activity on PtAu alloy nanoparticles. The enhanced ORR activity was attributed to enrichment of surface Pt, which led to weaker OH adsorption as well as a higher Pt surface area. Since the properties and optimum structure of surface alloys have been well established through computational simulations, this strategy (CO induced segregation) could be expended to other Pt alloy surfaces to improve ORR activity. This finding suggests that CO induced surface segregation could be used to enhance the catalytic activity of the carbon-supported alloy nanoparticles without changing the total composition.

4. Conclusions

We investigated the changes in ORR activity during CO induced surface Pt segregation in PtAu nanoparticles. Improved ORR activity on CO treated PtAu nanoparticles originated from enhancement of specific activity (1.12 mA cm_{Pt}^{-2} → 1.74 mA cm_{Pt}^{-2}) as well as increase of ECA_{Pt} (33.0 $cm^2 g_{Pt}^{-1}$ → 38.2 $cm^2 g_{Pt}^{-1}$). The Pt surface enrichment in PtAu-CO, which was determined through the XPS and electrochemical measurements, provided more active sites, ECA_{Pt}, for ORR, while the Ar treatment led to a 5% decrease in ECA_{Pt} when compared to PtAu-AP. The enhancement of specific activity on the Pt rich surface (PtAu-CO) was attributed to weaker adsorption energy of OH, which was confirmed by the positive shift of the pztc (12 mV) in the CO treated catalyst.

Acknowledgements

This research was supported by WCU (World Class University) program (R31-10013) through the National Research Foundation

of Korea funded by the Ministry of Education, Science and Technology and by the Joint Research Project funded by the Korea Research Council of Fundamental Science & Technology as a part of the "Development and mechanism study of high performance and durable components for high-temperature PEMFCs" (Seed-10-2). The work at Kookmin University was supported by Priority Research Centers Program through NRF funded by MEST (2009-0093814).

Appendix A. Supplementary data

Supplementary data associated with this article can be found, in the online version, at http://dx.doi.org/10.1016/j.apcatb.2012.09.041.

References

[1] V.R. Stamenkovic, B. Fowler, B.S. Mun, G. Wang, P.N. Ross, C.A. Lucas, N.M. Marković, Science 315 (2007) 493–497.
[2] S.J. Yoo, S.K. Kim, T.Y. Jeon, S.J. Hwang, J.G. Lee, S.C. Lee, K.S. Lee, Y.H. Cho, Y.E. Sung, T.H. Lim, Chemical Communications 47 (2011) 11414–11416.
[3] Y.H. Cho, T.Y. Jeon, J.W. Lim, Y.H. Cho, M. Ahnb, N. Jung, S.J. Yoo, W.S. Yoon, Y.E. Sung, International Journal of Hydrogen Energy 36 (2011) 4394–4399.
[4] Y. Sung, J. Hwang, J.S. Chung, International Journal of Hydrogen Energy 36 (2011) 4007–4014.
[5] V. Di Noto, E. Negro, Electrochimica Acta 55 (2010) 7564–7574.
[6] V. Di Noto, E. Negro, Fuel Cells 10 (2010) 234–244.
[7] Y. Ma, P.B. Balbuena, Journal of Physical Chemistry C 112 (2008) 14520–14528.
[8] J. Greeley, J.K. Nørskov, Electrochimica Acta 52 (2007) 5829–5836.
[9] V.R. Stamenkovic, B.S. Mun, K.J.J. Mayrhofer, P.N. Ross, N.M. Markovic, Journal of the American Chemical Society 128 (2006) 8813–8819.
[10] Y. Zhang, Q. Huang, Z. Zou, J. Yang, W. Vogel, H. Yang, Journal of Physical Chemistry C 114 (2010) 6860–6868.
[11] P. Hernández-Fernández, S. Rojas, P. Ocón, J.L.G. De La Fuente, J.S. Fabián, J. Sanza, M.A. Peña, F.J. García-García, P. Terreros, J.L.G. Fierro, Journal of Physical Chemistry C 111 (2007) 2913–2923.
[12] M.I. Awad, M.S. El-Deab, T. Ohsaka, Journal of the Electrochemical Society 154 (2007) B810–B816.
[13] G. Chen, Y. Li, D. Wang, L. Zheng, G. You, C.J. Zhong, L. Yang, F. Cai, J. Cai, B.H. Chen, Journal of Power Sources 196 (2011) 8323–8330.
[14] I.S. Park, K.S. Lee, J.H. Choi, H.Y. Park, Y.E. Sung, Journal of Physical Chemistry C 111 (2007) 19126–19133.
[15] N. Kristian, Y. Yu, P. Gunawan, R. Xu, W. Deng, X. Liu, X. Wang, Electrochimica Acta 54 (2009) 4916–4924.
[16] J. Huang, H. Hou, T. You, Electrochemistry Communications 11 (2009) 1281–1284.
[17] J. Wang, D.F. Thomas, A. Chen, Chemical Communications (2008) 5010–5012.
[18] J.H. Choi, K.W. Park, I.-S. Park, K. Kim, J.S. Lee, Y.-E. Sung, Journal of the Electrochemical Society 153 (2006) A1812–A1817.
[19] C.-W. Liu, Y.-C. Wei, K.-W. Wang, Journal of Colloid and Interface Science 336 (2009) 654–657.
[20] Y. Ma, H. Zhang, H. Zhong, T. Xu, H. Jin, X. Geng, Catalysis Communications 11 (2010) 434–437.
[21] B. Brown, S.D. Wolter, B.R. Stoner, J.T. Glass, Journal of the Electrochemical Society 155 (2008) B852–B859.
[22] E. Irissou, F. Laplante, S. Garbarino, M. Chaker, D. Guay, Journal of Physical Chemistry C 114 (2010) 2192–2199.
[23] B.N. Wanjala, J. Luo, B. Fang, D. Mott, C.-J. Zhong, Journal of Materials Chemistry 21 (2011) 4012–4020.
[24] B.N. Wanjala, J. Luo, R. Loukrakpam, B. Fang, D. Mott, P.N. Njoki, M. Engelhard, H.R. Naslund, J.K. Wu, L. Wang, O. Malis, C.-J. Zhong, Chemistry of Materials 22 (2010) 4282–4294.
[25] J. Luo, M.M. Maye, V. Petkov, N.N. Kariuki, L. Wang, P. Njoki, D. Mott, Y. Lin, C.-J. Zhong, Chemistry of Materials 17 (2005) 3086–3091.
[26] Y. Xing, Y. Cai, M.B. Vukmirovic, W.P. Zhou, H. Karan, J.X. Wang, R.R. Adzic, Journal of Physical Chemistry Letters 1 (2010) 3238–3242.
[27] M. Shao, A. Peles, K. Shoemaker, M. Gummalla, P.N. Njoki, J. Luo, C.J. Zhong, Journal of Physical Chemistry Letters 2 (2011) 67–72.
[28] J.K. Norskov, J. Rossmeisl, A. Logadottir, L. Lindqvist, J.R. Kitchin, T. Bligaard, H. Jonsson, Journal of Physical Chemistry B 108 (2004) 17886–17892.
[29] J. Greeley, M. Mavrikakis, Catalysis Today 111 (2006) 52–58.
[30] K.J.J. Mayrhofer, V. Juhart, K. Hartl, M. Hanzlik, M. Arenz, Angewandte Chemie International Edition 48 (2009) 3529–3531.
[31] G. Frens, Nature Physical Science 241 (1973) 20–22.
[32] I.-S. Park, K.-S. Lee, D.-S. Jung, H.-Y. Park, Y.-E. Sung, Electrochimica Acta 52 (2007) 5599–5605.
[33] Y. Jin, Y. Shen, S. Dong, Journal of Physical Chemistry B 108 (2004) 8142–8147.
[34] I.-S. Park, K.-S. Lee, J.-H. Choi, H.-Y. Park, Y.-E. Sung, Journal of Physical Chemistry C 111 (2007) 19126–19133.
[35] U.A. Paulus, T.J. Schmidt, H.A. Gasteiger, R.J. Behm, Journal of Electroanalytical Chemistry 495 (2001) 134–145.
[36] V. Climent, N. García-Araez, E. Herrero, J. Feliu, Russian Journal of Electrochemistry 42 (2006) 1145–1160.
[37] V. Climent, G.A. Attard, J.M. Feliu, Journal of Electroanalytical Chemistry 532 (2002) 67–74.
[38] J. Greeley, M. Mavrikakis, Nature Materials 3 (2004) 810–815.
[39] H.L. Skriver, N.M. Rosengaard, Physical Review B 46 (1992) 7157–7168.
[40] V.K. Kumikov, K.B. Khokonov, Journal of Applied Physics 54 (1983) 1346–1350.
[41] E. Rach, J. Heitbaum, Electrochimica Acta 32 (1987) 1173–1180.
[42] S.E. Hörnström, L. Johansson, A. Flodström, R. Nyholm, J. Schmidt-May, Surface Science 160 (1985) 561–570.
[43] F. Tao, M.E. Grass, Y. Zhang, D.R. Butcher, J.R. Renzas, Z. Liu, J.Y. Chung, B.S. Mun, M. Salmeron, G.A. Somorjai, Science 322 (2008) 932–934.
[44] M. Yin, Y. Huang, L. Liang, J. Liao, C. Liu, W. Xing, Chemical Communications 47 (2011).
[45] K.-W. Wang, S.-R. Chung, C.-W. Liu, Journal of Physical Chemistry C 112 (2008) 10242–10246.
[46] J.J. Yeh, I. Lindau, Atomic Data and Nuclear Data Tables 32 (1985) 1–155.
[47] W.M. Riggs, C.D. Wagner, L.E. Davis, J.F. Moulder, G.E. Muilnenberg, Handbook of X-ray Photoelectron Spectroscopy: A Reference Book of Standard Data for Use in X-ray Photoelectron Spectroscopy, Physical Electronics Division, Perkin-Elmer Corp., Eden Prairie, 1979.
[48] A.J. Bard, L.R. Faulkner, Electrochemical Methods: Fundamentals and Applications, 2nd ed., John Wiley & Sons, Inc., New York, 2001.
[49] M. Shao, A. Peles, K. Shoemaker, M. Gummalla, P.N. Njoki, J. Luo, C.-J. Zhong, Journal of Physical Chemistry Letters 2 (2010) 67–72.
[50] Y.H. Fang, Z.P. Liu, Journal of Physical Chemistry C 115 (2011) 17508–17515.
[51] Z. Peng, H. Yang, Nano Today 4 (2009) 143–164.
[52] R. Gómez, V. Climent, J.M. Feliu, M.J. Weaver, Journal of Physical Chemistry B 104 (1999) 597–605.
[53] G.A. Attard, O. Hazzazi, P.B. Wells, V. Climent, E. Herrero, J.M. Feliu, Journal of Electroanalytical Chemistry 568 (2004) 329–342.
[54] C. Angel, Surface Science 572 (2004) 11–22.
[55] B. Alvarez, V. Climent, A. Rodes, J.M. Feliu, Physical Chemistry Chemical Physics 3 (2001) 3269–3276.
[56] U.W. Hamm, D. Kramer, R.S. Zhai, D.M. Kolb, Journal of Electroanalytical Chemistry 414 (1996) 85–89.
[57] T. Sergio, Journal of Electroanalytical Chemistry and Interfacial Electrochemistry 33 (1971) 351–378.
[58] M.J. Weaver, Langmuir 14 (1998) 3932–3936.
[59] K.J.J. Mayrhofer, D. Strmcnik, B.B. Blizanac, V. Stamenkovic, M. Arenz, N.M. Markovic, Electrochimica Acta 53 (2008) 3181–3188.
[60] M.Ø. Pedersen, S. Helveg, A. Ruban, I. Stensgaard, E. Lægsgaard, J.K. Nørskov, F. Besenbacher, Surface Science 426 (1999) 395–409.